American Mineralogist, Volume 95, pages 1765–1772, 2010

Crystal structure of hydrous wadsleyite with 2.8% H_2O and compressibility to 60 GPa

Yu Ye,[1,*] Joseph R. Smyth,[2] Anwar Hushur,[3] Murli H. Manghnani,[3] Dayana Lonappan,[3] Przemyslaw Dera,[4] and Daniel J. Frost[5]

[1]Department of Physics, University of Colorado, Boulder, Colorado 80309, U.S.A.
[2]Department of Geological Sciences, University of Colorado, Boulder, Colorado 80309, U.S.A.
[3]Hawaii Institute of Geophysics, University of Hawaii, Honolulu, Hawaii 96822, U.S.A.
[4]Center for Advanced Radiation Sources, University of Chicago, Argonne National Laboratory, Argonne, Illinois 60439, U.S.A.
[5]Bayerisches Geoinstitut, Universität Bayreuth, Bayreuth D95440, Germany

Abstract

Hydrous wadsleyite (β-Mg_2SiO_4) with 2.8 wt% water content has been synthesized at 15 GPa and 1250 °C in a multi-anvil press. The unit-cell parameters are: a = 5.6686(8), b = 11.569(1), c = 8.2449(9) Å, β = 90.14(1)°, and V = 540.7(1) Å^3, and the space group is $I2/m$. The structure was refined in space groups *Imma* and $I2/m$. The room-pressure structure differs from that of anhydrous wadsleyite principally in the increased cation distances around O1, the non-silicate oxygen. The compression of a single crystal of this wadsleyite was measured up to 61.3(7) GPa at room temperature in a diamond anvil cell with neon as pressure medium by X-ray diffraction at Sector 13 at the Advanced Photon Source, Argonne National Laboratory. The experimental pressure range was far beyond the wadsleyite-ringwoodite phase-transition pressure at 525 km depth (17.5 GPa), while a third-order Birch-Murnaghan equation of state (EoS) [V_0 = 542.7(8) Å^3, K_{T0} = 137(5) GPa, K' = 4.6(3)] still fits the data well. In comparison, the second-order fit gives V_0 = 542.7(8) Å^3, K_T = 147(2) GPa. The relation between isothermal bulk modulus of hydrous wadsleyite K_{T0} and water content C_{H2O} is: K_{T0} = 171(1)–12(1) C_{H2O} (up to 2.8 wt% water). The axial-compressibility β_c is larger than both β_a and β_b, consistent with previous studies and analogous to the largest coefficient of thermal expansion along the c-axis.

Keywords: Compressibility, hydrous wadsleyite, neon, orthorhombic

Introduction

Wadsleyite dominates the mineralogy of the upper transition zone with pyrolite composition (Anderson 2007; Ringwood 1976) (up to 70 vol%). From a depth of 410 to 525 km downward, wadsleyite transforms to ringwoodite. Smyth (1987, 1994) predicted that wadsleyite can contain up to 3.3 wt% H_2O, because O1, the under-bonded non-silicate oxygen, is a likely site for hydration. Subsequently, Inoue et al. (1995) synthesized pure-magnesium hydrous wadsleyite with 3.1 wt% H_2O. The huge amount of water potentially incorporated into these silicate minerals in the mantle implies that the mass of liquid-water equivalent stored or recycled through the mantle might amount to several oceans. Such implications are important for the understanding of the evolution of crust and mantle and changes of ocean levels in the geological past (Drake and Righter 2002; Bercovici and Karato 2003).

Hydrogen in the wadsleyite structure has significant effects on the physical properties such as thermal expansion (Ye et al. 2009; Inoue et al. 1995) and compressibility (Holl et al. 2008). Inoue et al. (1995) studied the thermal expansion of hydrous wadsleyite (Mg_2SiO_4) with as much as 2.6 wt% H_2O, by powder X-ray diffraction up to 973 K at ambient pressure. Yusa and Inoue (1997) reported the compressibility of hydrous wadsleyite (Mg_2SiO_4) with 2.5 wt% H_2O, by powder X-ray diffraction to 8.5 GPa. Hazen et al. (2000) and Holl et al. (2008) have also reported K_{T0} up to 10 GPa. We have synthesized hydrous wadsleyite, with about 2.8 wt% H_2O, and refined its crystal structure at ambient conditions to obtain information on the hydration mechanism. We also measured the unit-cell parameters up to 61.3 GPa by single-crystal X-ray diffraction in a diamond anvil cell using neon as pressure medium at Sector 13 of the Advanced Photon Source (GSECARS).

Anhydrous wadsleyite crystallizes in the orthorhombic space group *Imma*. Hydration causes a volume expansion of the unit cell together with an apparent decrease in symmetry to monoclinic space group $I2/m$. Smyth et al. (1997) reported an iron-bearing wadsleyite with 2.3 wt% H_2O and β = 90.4°; Jacobsen et al. (2005) observed β up to 90.125(3)° for a sample with 1.06 wt% H_2O; Holl et al. (2008) described the sample with 1.66 wt% H_2O and β = 90.090(7)°. In this study, the monoclinic structure was further studied with respect to even higher water content.

Experimental methods and results

Synthesis

Crystals of hydrous pure Mg wadsleyite for this study were synthesized at 15 GPa and 1250 °C using a 2 mm welded Pt capsule in an 18 mm sintered MgO octahedron assembly in the 5000 ton multi-anvil press at Bayerisches Geoinstitut. Corner truncations on the 54 mm WC cubes were 8 mm and the heating duration time was 210 min. Starting material was synthetic anhydrous forsterite plus brucite and silica (quartz) to give a composition with 5.5 wt% H_2O. Single crystals up to 250 μm were obtained. No phases other than wadsleyite were noted in the capsule.

* E-mail: yey@colorado.edu

Unit-cell parameters

A single crystal about 120 × 100 × 70 μm³ in size was selected for structure and unit-cell refinement. Measurements for unit-cell refinements were carried out on a Bruker P4 four-circle diffractometer with a dual scintillation point detector system using an 18 kW rotating Mo-anode X-ray generator operated at 50 kV and 250 mA. Mo$K\alpha_1$-Mo$K\alpha_2$ mixed characteristic wavelength was used, and a single crystal of anhydrous forsterite with spherical shape was used to calibrate $K\alpha$(mix) = 0.71063 Å. $K\alpha$(mix) was used for cell refinements. The two-theta range was from 12 to 30°. After centering of all reflections, a least-squares fitting was done to calculate the cell parameters with uncertainties. Ninety reflections from the single crystal were centered to refine cell parameters with both a monoclinic and orthorhombic model. The refined monoclinic cell is a = 5.6686(8), b = 11.569(1), c = 8.2449(9) Å, β = 90.14(1)°, and V = 540.7(1) Å³; and the orthorhombic cell is a = 5.662(1), b = 11.577(2), c = 8.242(2) Å, and V = 540.3(2) Å³.

Crystal structure

Intensity data were collected using a Bruker APEX II CCD detector mounted on a P4 diffractometer. Refinements of atom positions and anisotropic displacement parameters were done using the program SHELXL-97 (Sheldrick 1997) in the software package WinGX (Farrugia 1999). We used scattering factors of Mg^{2+} and Si^{4+} reported by Cromer and Mann (1968), and those of O^{2-} from Tokonami (1965). XtalDraw (Downs et al. 1993) was used to calculate the bond lengths and polyhedral coordination parameters. To refine the structure, 6308 diffracted intensities (1179 unique) were measured with 2θ up to 88°. The structure was refined in the space groups *Imma* (orthorhombic) and *I*2/*m* (monoclinic). The orthorhombic structure refinement converged to R_{int} = 0.0339 and R_1 = 0.0361 for 984 unique reflections with $F_o > 4\sigma$, and 0.0421 for all 1136 unique reflections. The monoclinic structure refinement converged to R_{int} = 0.0305; and R_1 = 0.0360 for 1634 unique reflections with $F_o > 4\sigma$, and 0.0447 for all 1975 data. The refined atomic positions and site occupancy factors are listed in Table 1 for both orthorhombic and monoclinic structure refinements. CIFs are on deposit[1]. When the space group was changed from *Imma* to *I*2/*m*, the origin was shifted to (¼, ¼, ¼), and the x coordinates of Mg2, Si, O1, O2, and O3 were refined, instead of being fixed to 0. The Mg3 site splits into two non-equivalent sites: Mg3A (¼, 0.121, ¼) and Mg3B (¾, 0.379, ¼). Correspondingly, O4 also splits into two non-equivalent sites: O4A that is bonded to Mg3A, and O4B that is bonded to Mg3B. After adding H atoms, we found most of the cation vacancies on the Mg3 sites. This is consistent with the refinements of Holl et al. (2008) and Deon et al. (2010). These vacancies accounted for nearly 20% of the Mg3 sites, as indicated in Table 1, whereas nearly full occupancies were observed on Mg1, Mg2, and Si. All atoms were refined with anisotropic displacement parameters (Table 2). There were no significant differences between the two sets of displacement parameters. The bond lengths, polyhedral parameters, and edge lengths of cation polyhedra are listed in Table 3. Selected bond distances from this study (for *Imma* structure refinement) are compared to those for sample WS3056 with 0.005 wt% H_2O from Holl et al. (2008) in Table 4.

High-pressure XRD

High-pressure XRD experiments were conducted at beamline 13-BM-D, at GSECARS, Advanced Photon Source (APS), Argonne National Laboratory. The size of the single crystal for the high-pressure measurement was about 45 × 35 × 20 μm³. We used a symmetric piston-cylinder type diamond anvil cell (DAC), with 300 μm culets. The diamond cell was fitted with cubic boron nitride (cBN) seat on the downstream side, and hexagonal tungsten carbide (hWC) seat on the upstream side. A rhenium gasket, pre-indented to initial thickness of 30 μm, with a 165 μm diameter hole was used for the experiment. The DAC was loaded with neon as pressure medium using the COMPRES/GSECARS gas-loading system (Rivers et al. 2008). The pressure inside the cell was about 1.5 GPa after closing, and the gasket-hole diameter decreased by about 30%. Throughout the experiment, we used monochromatic synchrotron radiation with wavelength: λ = 0.3344 Å. An annealed ruby sphere placed in the sample chamber along with the sample served as the pressure marker.

For the high-pressure measurement, the diffractometer is a simple high-precision 1-axis rotation stage, and the detector was a MAR345 image plate, working in the low-resolution mode with a pixel size of 0.150 mm. The single-crystal diffraction data collection involved measuring three separate ω-oscillation images ("center," "left," and "right") at each pressure point: –13.5 to 15.5° with 5 min for "center" image, –30 to –19° with 2 min for "left" image, and 19 to 30° with 2 min for "right" image. The gaps in the rotation between these image ranges were omitted because of strong powder diffraction from hWC (on the upstream side) caused by the only partially absorbed transmitted X-ray beam. To obtain the orientation matrix at the initial pressure of 1.55 GPa, an ω step scan was performed in the range from –13.5 to 15.5°, with the step size of 1° and exposure time of 1

TABLE 2. Anisotropic displacement parameters

Cation	Param.	*Imma*	*I*2/*m*	Anion	Param.	*Imma*	*I*2/*m*
Mg1	U_{11}	0.0200(3)	0.0201(3)	O1	U_{11}	0.0086(4)	0.0201(3)
	U_{22}	0.0081(3)	0.0080(2)		U_{22}	0.0129(5)	0.0080(2)
	U_{33}	0.0184(3)	0.0190(3)		U_{33}	0.0122(5)	0.0190(3)
	U_{23}	0.0033(2)	0.0035(2)		U_{23}	0	0.0035(2)
	U_{13}	0	0.0017(2)		U_{13}	0	0.0017(2)
	U_{12}	0	0.0058(2)		U_{12}	0	0.0157(2)
	U_{eq}	0.0155(2)	0.0157(2)		U_{eq}	0.0112(2)	0.0113(2
Mg2	U_{11}	0.0124(2)	0.0124(2)	O2	U_{11}	0.0086(4)	0.0086(3)
	U_{22}	0.0063(2)	0.0061(2)		U_{22}	0.0129(5)	0.0130(4)
	U_{33}	0.0083(2)	0.0083(2)		U_{33}	0.0122(5)	0.0124(4)
	U_{23}	0	0		U_{23}	0	0
	U_{13}	0	–0.000(2)		U_{13}	0	0.0002(3)
	U_{12}	0	0		U_{12}	0	0
	U_{eq}	0.009(1)	0.009(1)		U_{eq}	0.0095(2)	0.0096(2)
Mg3A	U_{11}	0.0107(2)	0.0110(3)	O3	U_{11}	0.0117(3)	0.0116(3)
	U_{22}	0.0142(3)	0.0152(4)		U_{22}	0.0113(4)	0.0113(3)
	U_{33}	0.0092(3)	0.0099(3)		U_{33}	0.0087(3)	0.0090(3)
	U_{23}	0	0		U_{23}	0.0009(2)	0.0010(2)
	U_{13}	–0.0008(2)	–0.0007(2)		U_{13}	0	0.0000(2)
	U_{12}	0	0		U_{12}	0	0.0001(2)
	U_{eq}	0.0114(2)	0.0120(2)		U_{eq}	0.0106(2)	0.0107(2)
Mg3B	U_{11}	–	0.0106(3)	O4A	U_{11}	0.0097(2)	0.0096(2)
	U_{22}	–	0.0132(3)		U_{22}	0.0080(3)	0.0082(3)
	U_{33}	–	0.0084(3)		U_{33}	0.0101(3)	0.0103(3)
	U_{23}	–	0		U_{23}	0.0002(2)	0.0004(2)
	U_{13}	–	0.0004(2)		U_{13}	0.0004(2)	0.0004(2)
	U_{12}	–	0		U_{12}	0.0003(2)	0.0004(2)
	U_{eq}	–	0.0107(2)		U_{eq}	0.0093(2)	0.0094(2)
Si	U_{11}	0.0091(1)	0.0092(1)	O4B	U_{11}	–	0.0096(2)
	U_{22}	0.0076(2)	0.0075(1)		U_{22}	–	0.0079(3)
	U_{33}	0.0076(2)	0.0076(1)		U_{33}	–	0.0099(3)
	U_{23}	–0.00025(9)	–0.00024(7)		U_{23}	–	–0.0003(2)
	U_{13}	0	0.00003(8)		U_{13}	–	–0.0004(2)
	U_{12}	0	0.00002(7)		U_{12}	–	0.0002(2)
	U_{eq}	0.0081(1)	0.00811(9)		U_{eq}	–	0.0092(2)

[1] Deposit item AM-10-055, CIFs. Deposit items are available two ways: For a paper copy contact the Business Office of the Mineralogical Society of America (see inside front cover of recent issue) for price information. For an electronic copy visit the MSA web site at http://www.minsocam.org, go to the *American Mineralogist* Contents, find the table of contents for the specific volume/issue wanted, and then click on the deposit link there.

TABLE 1. Atomic position coordinates and occupancy factors

Imma					*I*2/*m*				
Atom	*x*/*a*	*y*/*b*	*z*/*c*	Occupancy	Atom	*x*/*a*	*y*/*b*	*z*/*c*	Occupancy
Mg1	0	0	0	0.984(4)	Mg1	0	0	0	0.984(3)
Mg2	0	0.25	0.97086(8)	0.994(4)	Mg2	0.0004(1)	0.25	0.97083(7)	0.992(3)
Mg3	0.25	0.12057(5)	0.25	0.804(7)	Mg3A	0.25	0.12052(6)	0.25	0.805(4)
					Mg3B	0.75	0.37937(5)	0.25	0.803(3)
Si	0	0.12120(3)	0.61531(4)	0.980(4)	Si	0.00003(5)	0.12119(2)	0.61532(3)	0.978(4)
O1	0	0.25	0.2260(2)	1.0	O1	–0.0000(2)	0.25	0.2261(1)	1.0
O2	0	0.25	0.7159(2)	1.0	O2	–0.0004(2)	0.25	0.7158(1)	1.0
O3	0	0.98671(8)	0.2563(1)	1.0	O3	–0.0002(1)	0.98671(7)	0.25640(8)	1.0
O4	0.2602(1)	0.12408(4)	0.99517(8)	1.0	O4A	0.2607(1)	0.12416(6)	0.99527(9)	1.0
					O4B	0.7402(1)	0.37597(6)	0.99526(9)	1.0

TABLE 3. Bond lengths (Å) and polyhedral parameters (Å) of cation polyhedra

		Imma	*I2/m*			*Imma*	*I2/m*
	Mg1				**Mg3B**		
	O3 ×2	2.118(1)	2.120(1)		O1 ×2	–	2.071(1)
	O4A ×4	2.058(1)	2.061(1)		O3 ×2	–	2.010(2)
	O4B	–	2.057(1)		O4B ×2	–	2.101(2)
O3	O4A(1)	3.055(2)	3.060(2)	O1	O1	–	2.862(2)
	O4A(2)	2.848(2)	2.849(2)		O3	–	3.056(2)
	O4B(1)	–	3.051(2)		O4B(1)	–	2.811(2)
	O4B(2)	–	2.852(2)		O4B(2)	–	3.045(2)
O4A	O4B(1)	2.874(2)	2.872(2)	O3	O3	–	2.834(2)
	O4B(2)	2.947(2)	2.951(2)		O4B(1)	–	3.051(2)
	Avg. bond	2.078(1)	2.079(2)		O4B(2)	–	2.929(2)
	Avg. edge	2.939(2)	2.938(2)		Avg. bond	–	2.091(2)
	Poly. V (Å^3)	11.898(5)	11.916(5)		Avg. edge	–	2.957(2)
					Poly. V (Å^3)	–	12.1002(6)
	Mg2				**Si**		
	O1	2.103(1)	2.104(1)		02	1.706(1)	1.705(1)
	O2	2.101(1)	2.102(1)		O3	1.637(1)	1.636(1)
	O4A ×4	2.081(2)	2.082(2)		O4A ×2	1.635(1)	1.637(1)
	O4B	–	2.084(2)		O4B	–	1.637(1)
O1	O4A	2.813(2)	2.818(2)	O2	O3	2.750(1)	2.748(1)
	O4B	–	2.811(2)		O4A	2.645(2)	2.647(2)
O2	O4A	3.097(2)	3.099(2)		O4B	–	2.644(2)
	O4B	–	3.100(2)	O3	O4A	2.714(2)	2.716(2)
O4A	O4B(1)	2.945(2)	2.951(2)		O4B	–	2.713(2)
	O4B(2)	2.916(2)	2.915(2)	O4A	O4B	2.716(2)	2.718(2)
	Avg. bond	2.089(1)	2.090(1)		Avg. bond	1.653(1)	1.654(1)
	Avg. edge	2.947(2)	2.949(2)		Avg. edge	2.697(2)	2.698(2)
	Poly. V (Å^3)	12.040(5)	12.054(5)		Poly. V (Å^3)	2.3088(4)	2.3102(4)
	Mg3A						
	O1 ×2	2.071(1)	2.071(1)				
	O3 ×2	2.010(2)	2.100(2)				
	O4A ×2	2.102(2)	2.102(2)				
O1	O1	2.859(2)	2.861(2)				
	O3	3.058(2)	3.056(2)				
	O4A(1)	2.813(2)	2.818(2)				
	O4A(2)	3.041(2)	3.037(2)				
O3	O3	2.833(2)	2.838(2)				
	O4A(1)	3.055(2)	3.060(2)				
	O4A(2)	2.927(2)	2.924(2)				
	Avg. bond	2.091(2)	2.091(2)				
	Avg. edge	2.957(2)	2.958(2)				
	Poly. V (Å^3)	12.1003(6)	12.1103(6)				

TABLE 4. Comparison of interatomic distances in wadsleyites with 0.005 and 2.8 wt% H_2O

C_{H2O} (wt% H_2O)	0.005	2.8 (for space group *Imma*)
Mg1-O3(2) (Å)	2.112(2)	2.118(1)
Mg1-O4(4) (Å)	2.050(1)	2.058(1)
Avg. bond (Å)	2.071(2)	2.078(1)
Poly. V (Å^3)	11.756(9)	11.898(5)
Mg2-O1(1) (Å)	2.029(4)	2.103(1)
Mg2-O2(1) (Å)	2.101(4)	2.101(1)
Mg2-O4(4) (Å)	2.092(1)	2.081(2)
Avg. bond (Å)	2.082(2)	2.089(1)
Poly. V (Å^3)	11.96(2)	12.040(5)
Mg3-O1(2) (Å)	2.018(1)	2.071(1)
Mg3-O3(2) (Å)	2.124(2)	2.010(2)
Mg3-O4(2) (Å)	2.131(2)	2.102(2)
Avg. bond (Å)	2.091(4)	2.091(2)
Poly. V (Å^3)	12.072(5)	12.1003(6)

min per image. The resulting 29 images were used to calculate ω angles for each reflection and the orientation matrix, as well as unit-cell parameters. This orientation matrix was then used as a first approximation to index peaks in images collected at subsequent pressures.

Pressure calibration

Ruby R_1 fluorescence line is widely used as pressure scale for high-pressure experiments in diamond anvil cells, with $\lambda_0 = 694.24$ nm for ambient pressure at 298 K (Silvera et al. 2007). Mao et al. (1986) calibrated the relationship between pressure and wavelength shift ($\Delta\lambda$) as in Equation 1 for "quasi-hydrostatic" argon to 80 GPa:

$$P_{Ar} = (A/B)\{[1 + (\Delta\lambda/\lambda)]^B - 1\} \text{ (GPa)} \quad (1)$$

where $A = 1904$ GPa and $B = 7.665$.

According to Dewaele et al. (2008), neon is a good quasi-hydrostatic pressure medium up to at least 80 GPa at room temperature, and the equation of state was reported in the pressure range up to 208 GPa, in which the crystal structure remained face-center-cubic. The diffraction patterns at 6, 12, 29, and 61 GPa are shown in Figures 1a–1d, created with software package GSE-ADA (Dera 2007a). Neon reflections were identified as short streaks, compared with the sharp reflection spots from the single crystal of hydrous wadsleyite and diamond. For each step above 12 GPa, neon reflections of (111), (200), and (220) could be observed on the 2D diffraction patterns, as indicated in Figures 1a–1d. Hence, for each step above 12 GPa, 6 to 8 reflection "streaks" from the diffraction patterns were used to calculate the pressure with statistical uncertainties, using the *PVT* equations of states from Fei et al. (2007) and Dorogokupets and Dewaele (2007). The pressure values read from the spectrometer and calculated from neon diffraction patterns are listed in Table 5.

In the following discussion and calculation, we have used the pressure values from neon diffraction patterns for the steps above 12 GPa. For the measurements below 12 GPa, the pressure values were derived from a spectrometer program that measured R_1 peak-shift and calibrated pressures on the basis of Equation 1, and we assume that the given values are of sufficient accuracy in the lower pressure range. Generally, the pressure values from neon diffraction patterns were slightly smaller than those from the ruby spectra. As pressure increased, the ruby moved to the edge of the gasket hole that may have caused the ruby to record slightly higher values than the crystal, due to the non-hydrostatic pressure from the edge of the gasket hole. In this study, we did not calibrate the ruby pressure scale in our neon pressure medium, because the uncertainties for pressures derived from neon diffraction patterns are larger than those from MgO volumes (Jacobsen et al. 2008), but still good enough to derive a reasonable value of K_{T0} as discussed below.

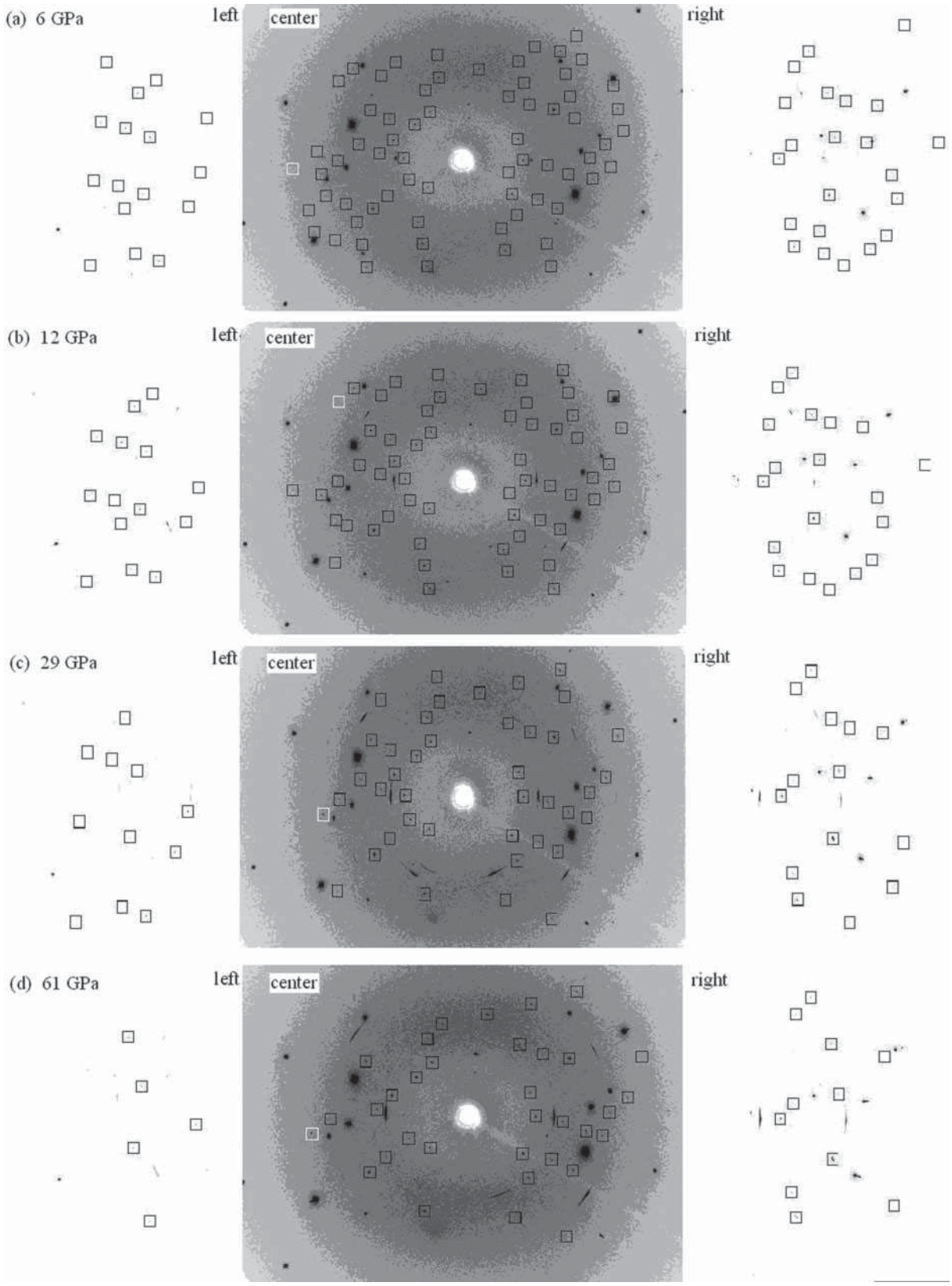

FIGURE 1. (**a**–**d**) The single-crystal diffraction patterns of "left," "center," and "right" images at the pressures of 6, 12, 29, and 61 GPa, respectively. The diffraction patterns from hydrous wadsleyite, which are used to calculate the unit-cell parameters, are marked with squares, and most of the unmarked strong reflection spots are from diamond. The neon reflection streaks appeared at 12 GPa, and became more apparent at 29 and 61 GPa. In **b**, the streaks on the inner rings are (111) streaks, the ones on the outer rings are (220). (200) streaks appeared in **c** and **d** between the rings for (111) and (220), although not as strong as (111) and (220) streaks.

TABLE 5. X-ray diffraction data for hydrous wadsleyite in neon pressure medium

P_{spect}† (GPa)	P_{neon}* (GPa)	*a* (Å)	*b* (Å)	*c* (Å)	*V* (Å³)
1.6(1)	–	5.656(6)	11.540(7)	8.221(4)	536.6(7)
2.9(2)	–	5.638(6)	11.516(7)	8.186(4)	531.5(7)
6.0(2)	–	5.612(7)	11.443(7)	8.131(4)	522.2(7)
12.1(2)	**11.8(2)**	5.544(8)	11.319(8)	8.032(5)	504.1(8)
14.6(2)	**14.8(4)**	5.522(8)	11.282(9)	7.985(5)	497.4(9)
17.5(4)	**17.1(2)**	5.51(1)	11.23(1)	7.940(7)	491(1)
20.2(3)	**19.6(2)**	5.50(1)	11.18(1)	7.904(7)	486(1)
23.0(4)	**22.5(4)**	5.46(1)	11.16(1)	7.865(7)	480(1)
25.7(6)	**25.0(5)**	5.439(7)	11.096(8)	7.852(5)	473.9(7)
29.5(4)	**28.9(5)**	5.413(8)	11.050(8)	7.804(5)	466.8(9)
32.7(3)	**31.7(7)**	5.391(8)	11.012(9)	7.775(5)	461.5(8)
36.4(5)	**35.5(5)**	5.379(7)	10.967(7)	7.734(5)	456.2(7)
40.5(2)	**39.6(5)**	5.351(9)	10.940(9)	7.703(6)	451.0(9)
45.6(4)	**45.0(4)**	5.32(1)	10.89(1)	7.639(8)	443(1)
51.7(2)	**50.8(4)**	5.28(1)	10.82(1)	7.600(7)	434(1)
55.6(3)	**55.1(5)**	5.26(1)	10.78(1)	7.563(6)	429(1)
61.2(2)	**61.3(7)**	5.24(1)	10.73(1)	7.515(7)	422(1)

Note: The pressure values used for further calculations are marked bold.
* P_{neon} values were determined from the equation of state of neon (Fei et al. 2007; Dorogokupets and Dewaele 2007).
† P_{spect} values were read from spectrometer, using the ruby fluorescence line calibrated by Mao et al. (1986). The uncertainty was determined by the difference between the values read before and after each measurement.

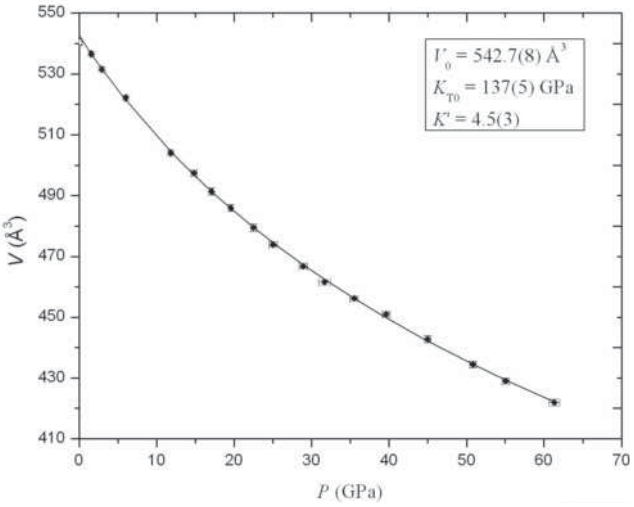

FIGURE 2. Plot of volume vs. pressure data with the fitting curve for the third-order B-M EOS. The calculated V_0, K_0, and K' are listed. The horizontal and vertical error bars represent pressure and volume uncertainties, respectively, if they are larger than the symbol sizes. The zero-pressure volume from our lab is marked as an open square symbol.

For each pressure, more than 50 reflections were used to refine the unit-cell parameters by the software packages of GSE-ADA (Dera 2007a) and RSV (Dera 2007b). The cell parameters, listed in Table 5, were calculated as orthorhombic unit cell. Because of the large uncertainties, we were unable to resolve a β-angle different from 90°. The program EoSFit (Angel 2001) was used to fit the pressure-volume data to the second- and third-order Birch-Murnaghan equations of state (B-M EOS). Volume vs. pressure are plotted in Figure 2, Birch normalized pressure (F_E) vs. Euler finite strain (f_E) are plotted in Figure 3, and *a*, *b*, and *c* axes compressions are plotted in Figures 4a–4c.

DISCUSSION

Water content and unit cell

Jacobsen et al. (2005) determined a relation between unit cell and water content for waddsleyite as:

$$b/a = 2.008(1) + 1.25(3) \times 10^{-6}\, C_{H_2O}\ (\text{ppm wt.}). \quad (2)$$

The water contents of samples WZ304, WH833, and WZ292 in that study were derived by the average of two values derived by the calibrations of Paterson (1982) and Libowitzky and Rossman (1997), respectively. However, Deon et al. (2010) published a new absorption coefficient for hydrous wadsleyite, which would give water contents about 20 wt% higher than those from Libowitzky and Rossman (1997). Calibration of the water contents of minerals from FTIR spectra is still an open problem with no absolute values yet, and each mineral seems to require its own calibration. Since Equation 2 is relatively well established and has been used in several studies, we use it here to calculate the water content of our sample for consistency with previous studies. We estimate an uncertainty of as much as 20% to cover any possible discrepancy caused by different calibration methods. The *b*/*a* ratio is 2.041 (2.63 wt% H_2O) for monoclinic structure, while 2.445 (2.92 wt% H_2O) for orthorhombic structure. Hence, we assume the water content to be the average of 2.8 wt% H_2O, with an uncertainty of 0.5 wt%.

The unit-cell parameters for current sample are consistent with the relationships of unit-cell parameters vs. water content in Figure 1 in Holl et al. (2008). For an increase of 1 wt% of H_2O, the *a* and *c* axes decrease by 0.20 and 0.05%, respectively; while the *b* axis and *V* increase by 0.40 and 0.16%, respectively. If we assume that vacancies only occur at Mg3 sites in the orthorhombic structure of hydrous wadsleyite (Deon et al. 2010), the density of the current sample should be 3.344(1) g/cm³, which is also consistent with Figure 2 in Holl et al. (2008).

Crystal structure

Selected interatomic distances from *Imma* structure refinements for the two samples are compared in Table 4. Relative to anhydrous wadsleyite, the Mg-O distances around O1 expand, whereas those around the other O atoms contract. In anhydrous wadsleyite, the O1 position is bonded only to five Mg atoms (four Mg3 and one Mg2) and thus is strongly under-bonded (Smyth 1987). Protonation of O1 relieves this imbalance, lengthens the bonds around O1, and permits the longer bonds around the other O atoms to contract. For the samples from Holl et al. (2008) and this study, the O1-O1, O1-O4, and O3-O3 edge lengths on M3 and O4-O4 edge length shared by M1 and M2 show a systematic decrease as water content increases. By extending the water content to 2.8 wt%, it further supports the claim by Smyth (1987) that O1, the non-silicate oxygen, is a preferred site for H in the structure, since H^+ cations have an effect of mitigating the repulsion between neighboring O^{2-} anions. The Mg1 and Si polyhedra from this study are about 0.4 and 0.3% larger, respectively, than those of SS0401, while the volumes of Mg2, Mg3A, and Mg3B polyhedra do not differ much. On the other hand, Deon et al. (2010) suggested that most protonation occurs along O1-O4 and O3-O4 edges of a vacant Mg3 octahedron, and the protonation is random with either two O1, two O3, or one O1 and one O3 in the vacant Mg3 octahedron. Slight splits for some reflection spots were observed on the diffraction patterns when intensity data were collected on the CCD detector, which supports the signs of strain due to polysynthetic twinning in the

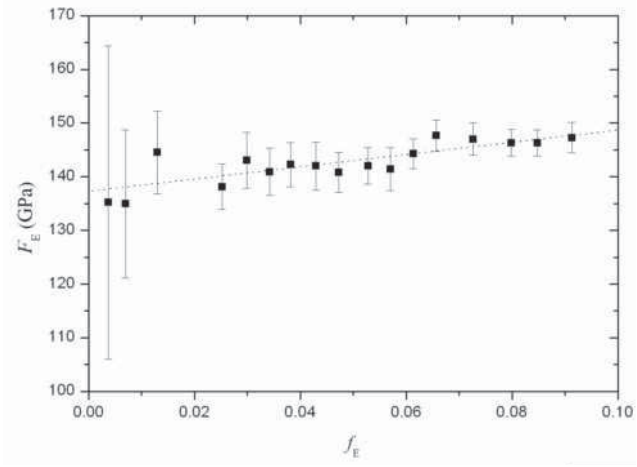

FIGURE 3. Birch normalized pressure (F_E) vs. Euler finite strain (f_E). The linear regressions gives the bulk modulus as *y*-intercept, and the positive slope shows that K' is larger than 4.

orthorhombic structure, noted by Holl et al. (2008).

In the structure refinement, several atoms are seen to deviate significantly from their equivalent positions in the orthorhombic structure. This split can be explained by the slight deviation of Mg2-O1 direction from the original direction, which had been perpendicular to the *a*-*b* plane. This could be induced by the protonation, since O1 is a preferable site for H atoms. In the O1 site tetrahedron, the observed distance from Mg2 to Mg3A and Mg3B are 3.087(2) and 3.093(2) Å, and the angles of Mg2-O1-Mg3A and Mg2-O1-Mg3B are 95.33(8) and 95.61(8)°, respectively. These differences are small but significant. Nevertheless, these distances and angles are identical for each Mg3 position in the orthorhombic structure. Hence, the Mg3A sites [(¼, 0.12, ¼) and (¼, 0.38, ¼)] were split from the Mg3B sites [(–¼, 0.12, ¼) and (–¼, 0.38, ¼)] along the direction of *a* axis, by the symmetry change, causing β to deviate slightly from 90°. We therefore refined the *x* coordinates in Table 1, to determine the splitting of the atom positions in the monoclinic structure.

Compression to 61.3 GPa

In a pyrolite composition model (Ringwood 1976; Anderson 2007), wadsleyite transforms to ringwoodite at about 525 km where T = 1790 K and P = 17.5 GPa. At 525 km depth, the density increases from 3.70 to 3.77 g/cm^3, and the adiabatic bulk modulus K_S increases from 231.9 to 249.5 GPa, whereas the bulk sound velocity $V_\Phi = (K_S/\rho)^{1/2}$ increases from 7.91 to 8.13 km/s (Yu et al. 2008). For better understanding of the compression mechanism of hydrous wadsleyite, we have investigated the room-temperature stability of hydrous wadsleyite up to 61.3 GPa, which is about three times higher than the pressure of the wadsleyite-ringwoodite phase transition at temperatures around 1800 K (Inoue et al. 2006; Kuroda et al. 2000; Suzuki et al. 2000). At room temperature, no phase change was observed because the kinetic energy is not high enough to overcome the barrier for the phase transition.

The calculated ambient condition unit-cell parameters from the third-order Birch-Murnaghan EoS are: a = 5.675(6), b = 11.592(8), c = 8.258(5) Å, and V = 542.7(8) Å^3. These values are

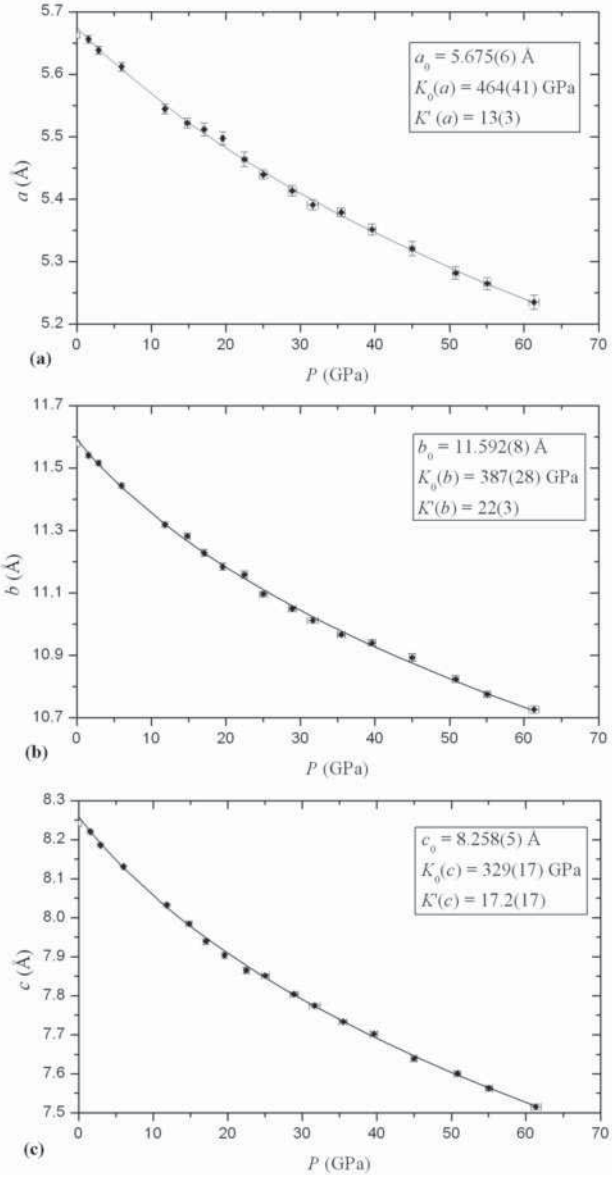

FIGURE 4. (**a**–**c**) The *a*-, *b*-, and *c*-axes compressions with fitting curves for third-order B-M EOS. The horizontal (pressure) and vertical (axes length) error bars are represented if they are larger than the symbol sizes. The zero-pressure axial lengths are marked as open square symbols.

larger than the ones measured in our lab, as indicated in Figures 2 and 4. This can be attributed to a systematic difference between the equipment in our lab and that at APS. However, the derived ambient condition *b*/*a* ratio is 2.043(3), which is in good agreement with the ratio value measured in our lab.

The best-fit parameters (V_0, K_{T0}, and K') from Birch-Murnaghan (B-M) EoS for the present study are listed in Table 6 together with other reported wadsleyite samples, and the ambient isothermal bulk modulus (K_{T0}) vs. water content is plotted in Figure 5 for the third-order B-M EOS. As can be seen, K_{T0} decreases as water content increases. The linear fitting gives the relation as (R^2 = 0.9498):

$$K_{T0}\ (\text{GPa}) = 171(1) - 12(1)\ C_{H_2O}\ (\text{wt\%}). \quad (3)$$

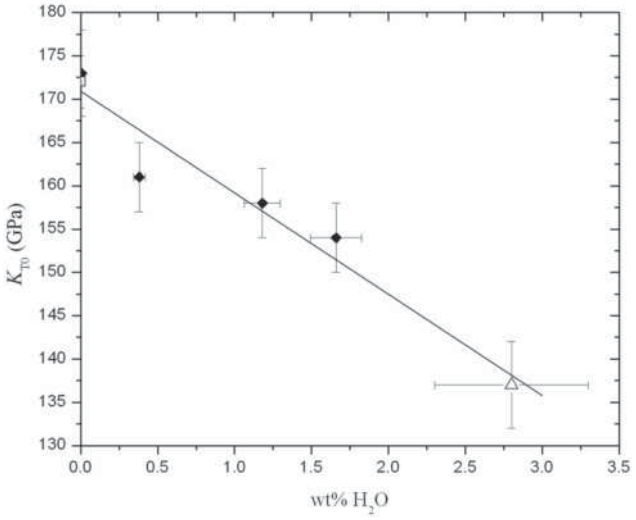

FIGURE 5. Plot of ambient K_{T0} vs. water content with linear fitting. The data are from Table 6 by the third-order B-M EOS [(0, 172) is from Hazen et al. (2000), (2.8, 137) is from the current study, and other data are from Holl et al. (2008)]. The errors for K_{T0} and water content are shown as vertical and horizontal error bars, respectively.

Isothermal bulk moduli K_T were generally derived from measuring high-pressure unit-cell volumes in diamond anvil cells by X-ray diffraction, while adiabatic moduli K_S were determined by elasticity measurements. The relationship between K_S and K_T is

$$K_T = K_S/(1 + \alpha\gamma T) \quad (4)$$

where α is thermal expansion coefficient (Inoue et al. 2004; Ye et al. 2009), γ is Grüneisen parameter (Chopelas 1991), and T is temperature in Kelvin.

Mean isothermal axial compressibility values of β_a, β_b, and β_c from this and previous studies are listed in Table 7. For the sample in the current study, the mean axial compressibility values calculated in the pressure range up to 14.8 GPa are larger than those in pressure range up to 6.13 GPa, because the isothermal axial β values will decrease when pressure increases. Nevertheless, the general trend shown in Table 7 indicates that β_a, β_b, and β_c all increase with increasing water content. Based on a single-crystal study, Ye et al. (2009) also reported that hydrous wadsleyite has larger α_a, α_b, and α_c than anhydrous one. Protonating the non-silicate O1 site will decrease bond strength around the vacant octahedron, resulting in a larger compressibility and thermal expansion (Ye et al. 2009). On the other hand, for each sample in Table 6, β_c is generally about 30 to 40% greater than β_a and β_b, and Zha et al. (1997) and Mao (2008a) reported that the longitudinal modulus C_{33} is smaller than C_{11} and C_{22} for their wadsleyite samples. In addition, Suzuki et al. (1980), Inoue et al. (2004), and Ye et al. (2009) each reported that the thermal expansion along the *c*-axis was greater than those parallel to *a* and *b* for anhydrous and hydrous samples. Evidence from compressibility and thermal expansion indicate that wadsleyite has the most flexibility in *c*-axis.

TABLE 6. Parameters for B-M equation of state, listed in the order of increasing water content

H_2O wt%	P_{max} (GPa)	V_0 (Å^3)	K_{T0} (GPa)	K'	Reference
0	10.12	539.26(9)	172(3)	6.3(7)	Hazen et al. (2000)
0	14.2		170(2)*	4.3(2)	Zha et al. (1997)
0	9.6		172(2)*	4.2(1)	Li et al. (1998)†
0.005	7.3	538.2(1)	173(5)	4(1)	Holl et al. (2008)
		538.2(1)	174(1)	4.0	
0.38	9.01	539.2(1)	161(4)	5(1)	Holl et al. (2008)
		539.1(2)	165(1)	4.0	Mao et al. (2008b)
0.84	12		160.3(7)*	4.1(1)	
1.18	8.56	539.8(1)	158(4)	4.2(9)	Holl et al. (2008)
		539.8(1)	159.2(8)	4.0	
1.66	9.58	540.6(2)	154(4)	5(1)	Holl et al. (2008)
		540.6(1)	160(1)	4	
2.5	8.5		155(2)	4.3	Yusa and Inoue (1997)
2.8	61.3	542.6(8)	137(5)	4.5(3)	This study
		541.6(6)	147(2)	4.0	

Note: V_0 values are given if they were refined in the references, and some of K' are listed without uncertainties if they were fixed, instead of being refined.
* Adiabatic bulk modulus.
† The sample is assumed to be anhydrous because no water content was reported, the formula is $(Mg_{0.88}Fe_{0.12})_2SiO_4$.

TABLE 7. Mean isothermal axial compressibilities of wadsleyite for some of the samples listed in Table 6, which were measured by static compression

H_2O wt%	β_a (10^{-3} GPa^{-1})	β_b (10^{-3} GPa^{-1})	β_c (10^{-3} GPa^{-1})	Reference
0	1.45(2)	1.46(3)	2.00(4)	Hazen et al. (2000)
0.005	1.55(4)	1.57(3)	2.22(2)	Holl et al. (2008)
0.38	1.66(4)	1.60(3)	2.21(3)	Holl et al. (2008)
1.18	1.64(5)	1.78(3)	2.30(3)	Holl et al. (2008)
1.64	1.48(9)	1.85(11)	2.21(3)	Holl et al. (2008)
2.5	1.67(3)	1.87(3)	2.32(4)	Yusa and Inoue (1997)
2.8	1.86(5)	1.83(8)	2.23(7)	This study (to 14.8 GPa)
2.8	1.32(5)	1.26(5)	1.52(6)	This study (to 61.3 GPa)

ACKNOWLEDGMENTS

This work was supported by U.S. National Science Foundation grant EAR 07-11165 (to J.R.S.) and EAR 05-38884 (to M.H.M.). Use of the IMCA-CAT beamline 13-BM-D at Advanced Photon Source was supported by the U.S. Department of Energy, Office of Science, Office of Basic Energy Sciences, under contract no. W-31-109-Eng-38.

REFERENCES CITED

Anderson, D.L. (2007) New Theory of the Earth. Cambridge University Press, U.K.

Angel, R.J. (2001) EoSFit, a program for fitting equations of state to *P-K-T* data. Version 5.2. Crystallography Laboratory, Virginia Tech, Blacksburg, Virginia.

Bercovici, D. and Karato, S. (2003) Whole-mantle convection and the transition-zone water filter. Nature, 425, 35–44.

Chopelas, A. (1991) Thermal properties of β-Mg_2SiO_4 at mantle pressures derived from vibrational spectroscopy: Implications for the mantle at 410 km depth. Journal of Geophysical Research, 96, 11817–11829.

Cromer, D.T. and Mann, J. (1968) X-ray scattering factors computed from numerical Hartree-Fock wave functions. Acta Crystallographica, A24, 321–325.

Deon, F., Koch-Müller, M., Rhede, D., Gottschalk, M., Wirth, R., and Thomas, S.-M. (2010) Location and quantification of hydroxyl in wadsleyite: New insights. American Mineralogist, 95, 312–322.

Dera, P. (2007a) GSE-ADA data analysis program for monochromatic single crystal diffraction with area detector. GeoSoilEnviroCARS, Argonne, Illinois.

——— (2007b) RSV reciprocal space viewer program for single crystal data analysis. GeoSoilEnviroCARS, Argonne, Illinois.

Dewaele, A., Datchi, F., Loubeyre, P., and Mezouar, M. (2008) High pressure-high temperature equations of state of neon and diamond. Physical Review B, 77, 094106.

Dorogokupets, P.I. and Dewaele, A. (2007) Equations of state of MgO, Au, Pt, NaCl-B1 and NaCl-B2: Internally consistent high-temperature pressure scales. High Pressure Research, 27, 431–436.

Downs, R.T., Bartelmehs, K.L., Gibbs, G.V., and Boisen, M.B. (1993) Interactive software for calculating and displaying X-ray or neutron powder diffractometer patterns of crystalline materials. American Mineralogist, 78, 1104–1107.

Drake, M.J. and Righter, K. (2002) Determining the composition of the Earth. Nature, 416, 39–44.
Farrugia, L.J. (1999) WinGX software package. Journal of Applied Crystallography, 32, 837–838.
Fei, Y., Ricolleau, A., Frank, M., Mibe, K., Shen, G., and Prakapenka, V. (2007) Toward an internally consistent pressure scale. Proceedings of the National Academy of Sciences, 104, 9182–9186.
Hazen, R.M., Weinberger, M.B., Yang, H., and Prewitt, C.T. (2000) Comparative high-pressure crystal chemistry of wadsleyite, β-$(Mg_{1-x}Fe_x)_2SiO_4$, with x = 0 and 0.25. American Mineralogist, 85, 770–777.
Holl, C.M., Smyth, J.R., Jacobsen, S.D., and Frost, D.J. (2008) Effects of hydration on the structure and compressibility of wadsleyite, β-(Mg_2SiO_4). American Mineralogist, 93, 598–607.
Inoue, T., Yurimoto, H., and Kudoh, Y. (1995) Hydrous modified spinel, $Mg_{1.75}SiH_{0.5}O_4$: A new water reservoir in the mantle transition region. Geophysical Research Letters, 22, 117–120.
Inoue, T., Tanimoto, Y., Irifune, T., Suzuki, T., Fukui, H., and Ohtaka, O. (2004) Thermal expansion of wadsleyite, ringwoodite, hydrous wadsleyite and hydrous ringwoodite. Physics of the Earth and Planetary Interiors, 143–144, 279–290.
Inoue, T., Irifune, T., Higo, Y., Sanehira, T., Sueda, Y., Yamada, A., Shinmei, T., Yamazaki, D., Ando, J., Funakoshi, K., and Utsumi, W. (2006) The phase boundary between wadsleyite and ringwoodite in Mg_2SiO_4 determined by in situ X-ray diffraction. Physics and Chemistry of Minerals, 33, 106–114.
Jacobsen, S.D., Demouchy, S., Frost, D.J., Boffa-Ballaran, T., and Kung, J. (2005) A systematic study of OH in hydrous wadsleyite from polarized FTIR spectroscopy and single-crystal X-ray diffraction: Oxygen sites for hydrogen storage in the Earth's interior. American Mineralogist, 90, 61–70.
Jacobsen, S.D., Holl, C.M., Adams, K.A., Fischer, R.A., Martin, E.S., Bina, C.R., Lin, J.F., Prakapenka, V.B., Kubo, A., and Dera, P. (2008) Compression of single-crystal magnesium oxide to 118 GPa and a ruby pressure gauge for helium pressure media. American Mineralogist, 93, 1823–1828.
Kuroda, K., Irifune, T., Inoue, T., Nishiyama, N., Miyashita, M., Funakoshi, K., and Utsumi, W. (2000) Determination of phase boundary between ilmenite and perovskite $MgSiO_3$ by in situ X-ray diffraction and quench experiments. Physics and Chemistry of Minerals, 27, 523–532.
Li, B., Liebermann, R.C., and Weidner, D. (1998) Elastic moduli of wadsleyite (β-Mg_2SiO_4) to 7 Gigapascals and 873 Kelvin. Science, 281, 675–677.
Libowitzky, E. and Rossman, G.R. (1997) An IR absorption calibration for water in minerals. American Mineralogist, 82, 1111–1115.
Mao, H.K., Xu, J., and Bell, P.M. (1986) Calibration of the ruby pressure gauge to 800 kbar under quasi-hydrostatic conditions. Journal of Geophysical Research, 91, 4673–4676.
Mao, Z., Jacobsen, S.D., Jiang, F., Smyth, J.R., Holl, C.M., and Duffy, T.S. (2008a) Single-crystal elasticity of wadsleyities, β-Mg_2SiO_4, containing 0.37–1.66 wt% H_2O. Earth and Planetary Science Letters, 266, 78–89.
——— (2008b) Elasticity of hydrous wadsleyite to 12 GPa: Implications for Earth's transition zone. Geophysical Research Letters, 35, L21305, doi: 10.1029/2008Ge035618.
Paterson, M. (1982) The determination of hydroxyl by infrared absorption in quartz, silicate glasses, and similar materials. Bulletin de Minéralogie, 105, 20–29.
Ringwood, A.E. (1976) The Chemical Compositions and Origin of the Earth, p. 287–356. Advances in the Earth Science, M.I.T. Press, Cambridge.
Rivers, M., Prakapenka, V.B., Kubo, A., Pullins, C., Holl, C.M., and Jacobsen, S.D. (2008) The COMPRES/GSECARS gas-loading system for diamond anvil cells at the Advanced Photon Source. High Pressure Research, 28, 273–292.
Sheldrick, G.M. (1997) SHELXL97, Release 97-2. Program for the refinement of crystal structures. University of Göttingen, Germany.
Silvera, I.F., Chijioke, A.D., Nellis, W.J., Soldatov, A., and Tempere, J. (2007) Calibration of the ruby pressure scale to 150 GPa. Physica Status Solidi (b), 244, 460–467.
Smyth, J.R. (1987) β-Mg_2SiO_4: A potential host for water in the mantle? American Mineralogist, 72, 1051–1055.
——— (1994) A crystallographic model for hydrous wadsleyite: An ocean the Earth's interior? American Mineralogist, 79, 1021–1025.
Smyth, J.R., Kawamoto, T., Jacobsen, S.D., Swope, R.J., Herving, R.L., and Holloway, J.R. (1997) Crystal structure of monoclinic hydrous wadsleyite. American Mineralogist, 82, 270–275.
Suzuki, I., Ohtani, E., and Kumazawa, M. (1980) Thermal expansion of modified spinel, β-Mg_2SiO_4. Journal of Physics of the Earth, 28, 273–280.
Suzuki, A., Ohtani, E., Morishima, H., Kubo, T., Kanbe, Y., Kondo, T., Okada, T., Terasaki, H., Kato, T., and Kikegawa, T. (2000) In situ determination of the boundary between wadsleyite and ringwoodite in Mg_2SiO_4. Geophysical Research Letters, 27, 803–806.
Tokonami, M. (1965) Atomic scattering factor for O^{2-}. Acta Crystallographica, 19, 486.
Ye, Y., Schwering, R.A., and Smyth, J.R. (2009) Effects of hydration on thermal expansion of forsterite, wadsleyite, and ringwoodite at ambient pressure. American Mineralogist, 94, 899–904.
Yu, Y.G., Wu, Z., and Wentzcovitch, R.M. (2008) α-β-γ transformations in Mg_2SiO_4 in Earth's transition zone. Earth and Planetary Science Letters, 273, 115–122.
Yusa, H. and Inoue, T. (1997) Compressibility of hydrous wadsleyite (β-phase) in Mg_2SiO_4 by high pressure X-ray diffraction. Geophysical Research Letters, 24, 1831–1834.
Zha, C.-S., Duffy, T.S., Mao, H.-K., Downs, R.T., Hemley, R.J., and Weidner, D.J. (1997) Single-crystal elasticity of β-Mg_2SiO_4, to the pressure of the 410 km seismic discontinuity in the Earth's mantle. Earth and Planetary Science Letters, 147, E9–E15.

MANUSCRIPT RECEIVED FEBRUARY 17, 2010
MANUSCRIPT ACCEPTED JULY 2, 2010
MANUSCRIPT HANDLED BY LARS EHM